Smoluchowski ripening and random percolation in epitaxial $Si_{1-x}Ge_x/Si(001)$ islands

R. Arief Budiman and Harry E. Ruda
Centre for Advanced Nanotechnology, University of Toronto, Toronto, Ontario M5S 3E3, Canada
(Received 25 August 2000; revised manuscript received 2 November 2001; published 3 January 2002)

Island size distributions of ripened $Si_{1-x}Ge_x/Si(001)$ ($x=0.3-0.7$) islands exhibit a slow decay at small island sizes and an asymmetric bell-shaped distribution peaked at a large size. We explain the ripening process in $Si_{1-x}Ge_x/Si(001)$ islands by proposing a model based on random percolation and Smoluchowski ripening. Drawing an analogy with percolation theory, we use a shifted average height to represent the time variable, which is also applicable in the Smoluchowski ripening model; this shifted average height is used to analyze size distributions and correlation functions. Critical exponents derived from the site percolation model at $d=3$ agree with our measurements. Island diffusion $D \propto s^{-\alpha}$ leading to coalescence events, shows a weak dependence on size s: $\alpha=0.28\pm0.20$, attributable to the inverse process of sequential incorporation of atoms at step edges due to the high stress concentration at island terrace perimeters. While random percolation dominates for small sizes regime, Smoluchowski ripening controls the distribution peak at large island sizes. Good agreement is obtained between the model and the measured island size distributions.

DOI: 10.1103/PhysRevB.65.045315 PACS number(s): 68.35.Bs, 64.60.Ak, 61.46.+w

I. INTRODUCTION

The submonolayer island size distribution[1–3] was found to agree with both submonolayer homoepitaxial Fe thin films[2] and submonolayer heteroepitaxial InAs/GaAs thin films,[4,5] although the latter works only for one orthogonal surface direction, since anisotropic growth effects cause a breakdown of the isotropic scaling assumption that underlies the submonolayer size distribution.[5] Nevertheless, the agreement demonstrates that during submonolayer deposition, the size statistics of two-dimensional (2D) islands (or sometimes referred to as platelets) reveals a generic behavior, irrespective of the magnitude of misfit strain due to lattice constant mismatch between substrate and film.

With increased submonolayer coverage, the individual 2D islands become eventually connected and form an incipient infinite-size platelet at some critical coverage called the first-layer percolation threshold $\theta_p<1$ monolayer (ML).[1] Figures 1(a) and 1(b) illustrate these submonolayer events. For coverages below θ_p, the submonolayer size distribution for random percolation is expected to decay exponentially with island size.[6] The exponential dependence appears as well in the submonolayer size distribution for Ref. 2. For coverages $\theta \approx \theta_p$, however, the size statistics of the 2D islands typically follows a power-law behavior[3] and may be described using random percolation model.[6]

It is not clear physically why the presence of elastic strains in the heteroepitaxial deposition does not significantly modify the generic behavior of the submonolayer size distribution. One possible explanation is that the absence of a wetting layer in the submonolayer deposition may inhibit an elastic island-island interaction, since the substrate typically has a higher modulus of rigidity than the film.[7] The elastic strains in the individual 2D islands are thus largely confined within each island.

The situation changes dramatically for multilayer epitaxial thin film growth (i.e., $\theta>1$ ML), where the first-layer percolation has occurred.[8] In Stranski-Krastanow (SK) growth, 3D islands form after a wetting layer of a few MLs is established. During formation of the wetting layer, the 2D first-layer percolation occurs for each deposition of 1 ML. With increased coverage, the elastic interaction is expected to become stronger due to the presence of the wetting layer and the concomitant increase in elastic energy.

3D islands will form in the SK mode when the coverage reaches a critical thickness (coverage) h_c for the 2D-3D island transition as shown schematically in Fig. 1(c). The critical thickness h_c is determined by a force balance between surface tension and misfit stress. While surface tension tends to keep the surface flat, thus pseudomorphically strained, bulk shear deformations that propagate to the film surface will introduce shape transformations. For $\theta>h_c$, the free energy drop from the elastic deformations will outweigh the energy cost of increased surface area. h_c has been shown to depend on the misfit strain ε, originating from the lattice constant difference between substrate a_s and film a_f, as $h_c \propto \varepsilon^{-n}$, where $\varepsilon=(a_s-a_f)/a_s<0$ for a compressive strain. Different dependencies of h_c on ε have been reported. $n=4$ was reported by Perović and co-workers,[9] while the ε^{-1} dependence was reported by Tromp and co-workers.[10] Earlier work on theory of thin film elastic instability showed that $h_c \propto \varepsilon^{-8}$.[11] There is still no wide agreement on the value of n. It is not surprising therefore that the connection between h_c and effects on island size distribution has been largely unexplored.

Here we show that h_c marks the change of island dimensionality: from 2D islands to 3D islands. For time-dependent studies of 3D island size distribution, h_c approximates the location of *time origin* for the 3D island evolution. The time invariance of the 3D size distribution should therefore be defined using h_c, such that the average 3D island size $S(t)$, for example, behaves as $S(t) \sim S(\langle h \rangle - h_c)$, where $\langle h \rangle$ is the mean surface height.

When 3D islands ripen, the ripening process may be regarded partially as a 3D percolation. The size distribution of random percolation for ripened islands is mathematically shown to be a subexponentially decaying function of island size.[6] These observations raise an important hypothesis of

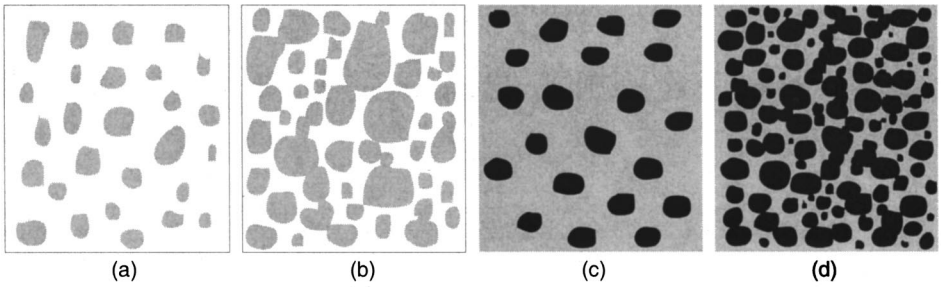

FIG. 1. (a) 2D platelets forming in a submonolayer film coverage ($\theta \lesssim \theta_p < 1$) before first-layer percolation occurs. White shading indicates a bare substrate. (b) The first-layer percolation occurs at $\theta \gtrsim \theta_p$ when an incipient infinite-size platelet emerges. Here the gray shading shows the first-layer growth. (c) After the first layer is deposited ($\theta > 1$), three-dimensional (3D) islands form at some critical coverage $h_c > 1$. Black shading shows the multilayer growth. (d) Eventually, these 3D islands will ripen by some coalescence mechanism, qualitatively resembling the first-layer percolation, but with $d=3$ instead of $d=2$. Due to the stress concentration around each 3D island perimeter, it is expected that the coalescence of 3D islands is governed by a random percolation process and some other mechanism(s).

whether a similarly good agreement may emerge between measured size distributions of ripened 3D islands and a 3D island size distribution with a random percolation component. The random percolation occurs when deposition flux ''floods'' the intervening wetting layer region between two 3D islands and thus connects them together. Intuitively, one can think of this random percolation as a noninteracting ''deposition-induced ripening.'' For a sufficiently small growth rate, the deposition-induced ripening should affect only smaller sized islands due to their small heights. In addition, there may also be an interacting component of 3D island ripening, which of course originates from some other mechanism. These interacting and noninteracting ripening processes mark the late growth stages of 3D islands as shown in Fig. 1(d).

In this paper, the island size distributions of ripened islands are analyzed using random percolation and coalescence mechanisms. The former mechanism describes the noninteracting coalescence events due to the incident deposition flux, and the latter describes the correlated coalescence events as islands diffuse and coalesce with each other. The random percolation and coalescence mechanisms are discussed in detail in Secs. II B and II C, respectively. We shall refer the correlated coalescence mechanism as Smoluchowski ripening as well, as its distribution function is obtained from Smoluchowski equation.[12]

The Ostwald ripening mechanism, in which ripening is due to the evaporation of atoms from smaller islands and their condensation onto larger islands, cannot describe the size distributions exhibited by $Si_{1-x}Ge_x/Si(001)$ islands we studied. This is further supported by the cellular (breath figure) network morphology found in our samples. The evaporation and condensation processes in Ostwald ripening demand intervening flat regions between islands to allow for adatoms to diffuse.[13] Under Ostwald ripening, islands should therefore be well separated, producing well-defined island topographies. Another reason why Ostwald ripening cannot be the ripening mechanism in our samples is the relatively narrow (about 3–4 orders of magnitude) size distribution predicted by Ostwald ripening;[13] our samples produced 6–7 orders of magnitude spread in their island size distributions. The nonoccurence of capillary-driven Ostwald ripening was also found in $Si_{0.8}Ge_{0.2}/Si(001)$ islands grown at 755 °C.[14]

To perform this analysis we first define several statistical measures, as described in Sec. II A, including the average island size S and number density n_s of islands per lattice site. Here the island size s is the island volume defined as the product of island base area and its average height. This definition allows for a more general shape of island geometry, which is important for calculating the volume of coalescing islands. Our main results are presented in Sec. III. Sections III A and III B discuss results from Smoluchowski ripening and random percolation components, respectively. In Sec. III C, we propose a general probability density function by incorporating these two mechanisms and we find good agreement with measured island size distributions. Section IV summarizes these results and discusses implications for predicting and controlling island size distributions.

II. MODEL

A. Statistical measures

To study the evolution of island size distributions, the island size definition should reflect the global height shift due to advancing growth front, as parametrized by the average comoving coordinate $\langle h \rangle \mapsto \langle h \rangle + Ft$, where $\langle h \rangle$ is the mean surface height and F is average constant growth rate. The comoving scheme naturally removes the infinite-size islands (i.e., the wetting layer) from the island size distributions. The island size s is defined as the island volume given by the product of island base area A and average island height $h_0 = A^{-1} \int (h - \langle h \rangle) dA$. The local surface height $h = h(\mathbf{x}, t)$ was measured using an atomic force microscope (AFM). Island base area is measured at the mean surface height $\langle h \rangle$ (i.e., the mean value from the height histogram from each AFM image). Although $\langle h \rangle$ can be roughly estimated from Ft, $\langle h \rangle \neq Ft$ since the deposited material distributes itself on the surface by forming islands of various sizes, and thus $\langle h \rangle$ depends on both the amount of deposited material and the surface height distribution. The equality $\langle h \rangle = Ft$ is true only for a flat surface. For simplicity, however, we assume $\langle h \rangle \approx Ft$ throughout.

The island size histogram is constructed by counting the number N of islands within a size interval $s_n \leqslant s \leqslant (s_n + \epsilon)$,

where $(s_n+\epsilon)$ is defined as the size bin in the nth interval of the histogram. Each interval has a width ϵ, and contains N number of islands. If the histogram covers a relatively narrow range, then the width ϵ can be defined as a constant. However, if the range is very wide, it is possible to scale the width to follow a geometric or logarithmic sequence. This is typical of our data.

When normalized with respect to the total number of islands, $\Omega=\Sigma_s N(s)$, each discrete point in the histogram gives the occupation probability $P_s(s)$ for an arbitrary site by an island of size $(s_n+\epsilon)$,

$$P_s(s,\theta)=\frac{N(s,\theta)}{\sum_s N(s,\theta)}, \tag{1}$$

where P_s also depends on the amount of deposited material θ, which in turn depends on time t given by $\theta=Ft$. Note, that P_s is already a spatially averaged probability density function, and thus independent of the coordinates **x**. The average island size S is therefore obtained from

$$S(\theta)=\sum_s sP_s, \tag{2}$$

following the standard definition for the average island size.[1,15] We note that the total number Ω of islands is a function of θ. We see from Eq. (1) that $\Omega=\Sigma_s N(s,\theta)$ may be viewed as a partition function in the language of statistical mechanics.

Experimentally, it is difficult to determine θ from Ft since the growth rate may fluctuate and growth termination does not occur instantaneously. In our case, for example, the nominal film thicknesses θ's are 5 and 20 nm, but the height histograms produce mean values ranging from 7.3 to 22.7 nm. Thus, we define

$$\theta\equiv\langle h\rangle, \tag{3}$$

as $\langle h\rangle$ is readily measurable from the AFM images. With this definition, the variables θ and $\langle h\rangle$ are interchangeable.

The number density, or island concentration, per lattice site for an island of size s is given by

$$n_s(s,\theta)=\frac{P_s}{s}, \tag{4}$$

and the kth moment of the size distribution is defined by

$$M_k(\theta)=\frac{\sum_s s^{k+1}P_s}{\sum_s s^k P_s} \quad \text{for} \quad k\geqslant 1, \tag{5}$$

in analogy with percolation theory.[6] We compute M_k to assess the dominance of random percolation over Smoluchowski ripening. This can be done since M_k should follow a certain behavior, as laid out in Sec. II B, if the distributions were dominated by random percolation.

B. Percolation distribution function and critical thickness

Random percolation in a lattice system describes coalescence (percolation) events of lattice sites or bonds when their site or bond probability p, respectively, is determinedy *randomly*, independent of the states of the neighboring sites or bonds.[6] In epitaxial thin film growth, the site or bond probability is equal to the probability of a surface site to be occupied by an incident particle. This probability is in turn proportional to the growth rate F. Percolation is said to occur at $p\approx p_p$ when a path connecting one end of the system to the other end emerges as p is increased to p_p. Since the incident particles coalesce and form an island, the connected path is analogous to an infinite-size island. For the submonolayer case, the 2D percolation occurs when the 2D islands are connected at the first-layer percolation threshold θ_p, thus we have $p_p\equiv\theta_p$.

Typical values for p_p for 2D percolation is 0.5–0.59. For bond percolation in a 2D square lattice (where edges connecting two nearest-neighbor sites are assigned a probability p to be open) the percolation threshold occurs at $p_p=\frac{1}{2}$,[6] while for site percolation (where each lattice site is assigned a probability p to be occupied) the corresponding value is $p_p\approx 0.59$.[16] Epitaxial thin film growth at an elevated temperature induces a surface diffusion field, which gives $p_p\approx 0.55-0.72$ ML for $R/F=10-10^6$, where the hop rate R of adatom is assumed to be proportional to the adatom diffusion length.[1,8] Thus, even for very large diffusion lengths, the percolation threshold in submonolayer epitaxial thin film growth does not significantly change from that of a 2D random site percolation problem.

In a random percolation process during submonolayer growth, the island size distribution at $\theta_p<\theta<1$ ML is provided by percolation theory. Specifically, it is assumed that the probability density function P_p in a percolation problem takes the following form:[6]

$$P_s(s)\sim\begin{cases} s^{-\sigma}f_-[s/\xi(p)^\tau] & \text{if } p\leqslant p_p, \\ s^{-\sigma}f_+[s/\xi(p)^\tau] & \text{if } p\geqslant p_p, \end{cases} \tag{6}$$

where σ and τ are positive constants, and $\xi(p)$ is a characteristic length scale. The scaling functions f_- and f_+ are for below and above the percolation threshold, respectively. A fundamental assumption in scaling theory is that there is a power law dependence of $\xi(p)$ on p:[6]

$$\xi(p)\approx|p-p_p|^{-\nu} \quad \text{as} \quad p\to p_p, \tag{7}$$

where ν is a positive (critical) exponent.

The applicability of the submonolayer island size distribution function[2] to the multilayer growth of *preripened* 3D InAs/GaAs islands[4] demonstrates the universality of the distribution function despite the change of island dimensionality from $d=2$ in submonolayer islands to $d=3$ in multilayer islands. The wetting layer beneath 3D InAs islands, therefore, does not change the nature of the distribution function. This implies that the distribution function $P_s(s)$ that satisfies the sum rules[1] $\int P_s(s)ds=1$ and $\int sP_s(s)ds=1$ must be defined by excluding the infinite-size island produced by either monolayer percolating 2D platelets in submonolayer growth, or by multilayer percolating 2D platelets in multilayer growth (i.e., the wetting layer). Hence, the island size s remains finite, i.e., $s<\infty$, such that the sum rules read as $\int_0^{<\infty}P_s(s)ds=1$ and $\int_0^{<\infty}sP_s(s)ds=1$ since $P_s(s)$ is limited

only for finite-size islands. The exclusion of wetting layer in the island size distribution further indicates that time during growth may be scaled by a shifted height variable with an appropriate height corresponding to the thickness of the wetting layer. We determined this thickness to be the critical thickness h_c.

Now we use our proposition that similar behavior may hold as well for ripened 3D islands, where $\theta > h_c$. Since the 3D islands form only after $\theta = h_c$, the following correspondence is postulated: $p_p \Leftrightarrow h_p \equiv (h_c + \theta_p)$. By defining $h_p \equiv h_c + \theta_p$, we have assumed that for ripening to occur, the coverage needs to be increased by θ_p once the 3D islands form at $\theta = h_c$. Thus, the percolation island size distribution function at $\theta > h_c$ is given by

$$P_s(s,\langle h\rangle) \sim s^{-\sigma} f[s/\xi(\langle h\rangle)^{\tau}], \tag{8}$$

where

$$\xi(\langle h\rangle) \approx |\langle h\rangle - h_p|^{-\nu} \text{ as } \langle h\rangle \to h_p. \tag{9}$$

f_+ is replaced by f in Eq. (8) since we consider only the ripening island size distribution, which corresponds to the $p > p_p$ case in the site percolation. This is because the wetting layer (i.e., a 3D infinite-size island) already forms beneath finite 3D islands. We further assume that there is a one-to-one correspondence between each critical exponent at $\theta_p < \theta < 1$ ML and that at $h > h_p$ for the same dimensionality. This is reasonable since the dimensionality d is the most important parameter in percolation for determining the critical exponents.[16] We can also express the probability density function P_s as follows:

$$P_s(s,\langle h\rangle) \sim s^{-\sigma} f(s^{1/(\nu\tau)} |\langle h\rangle - h_p|), \tag{10}$$

by rearranging the argument of $f(x)$ to conform with the conventions of percolation theory.[16]

The strict mapping between 3D random percolation and 3D small coherent islands introduced above requires that the mass distribution along the growth direction be statistically similar as found, e.g., in bulk 3D cluster growth. However, semiconductor islands typically develop into faceted structures, such as pyramids and domes for $Si_{1-x}Ge_x/Si(001)$ islands, thus breaking this statistical similarity. For this reason, it is expected that 3D random percolation would qualitatively capture only the scaling properties of relatively small sizes of unfaceted islands. Thus, in general, one would have to also consider the island shape and height distributions,[8] in addition to the size distributions.

We note here that all coverages θ reported by Ebiko and co-workers[4] obey $\theta < h_c + \theta_p$ with $\theta_p \approx 0.55$ to 0.72 ML (Ref. 1) and $h_c = 1.5-2$ ML's for InAs/GaAs islands,[17,18] ensuring that no ripening occurred. Coalescence of InAs/GaAs islands was definitely observed at $\theta = 3-4$ ML's.[19] We assume $\theta_p = 0.6$ ML in our analysis, corresponding to random site percolation in a 2D square lattice.

Finally, we emphasize that by using $\langle h\rangle$ as the base height of 3D islands in our island size definition, we assume that there is already an infinite-size cluster of height $\langle h\rangle - h_c$. This assumption is consistent with the AFM data as explained in Sec. III. Hence, the ripening island size distribution corresponds to an above-percolation-threshold case, i.e., $\langle h\rangle > h_p$.

C. Smoluchowski ripening distribution function

To analytically describe island ripening via coalescence, we consider coalescence events via pairwise collisions between two islands given by the Smoluchowski equation[20]

$$\frac{dn_s(t)}{dt} = \frac{1}{2}\sum_{s'} K(s', s-s') n_{s'}(t) n_{s-s'}(t) - n_s(t) \sum_{s'} K(s,s') n_{s'}(t), \tag{11}$$

where the kernel $K(s,s')$ defines the rate of collision between islands of sizes s and s'. The first term represents a density increase for islands of size s due to pairwise coalescence events between islands of sizes s' and $s-s'$. The second term represents a density decrease owing to coalescence events between islands of size s and islands of arbitrary sizes. It was shown that if the collision process is time-independent and homogeneous $K(\lambda s, \lambda s') = \lambda^{2\omega} K(s,s')$, and islands are spatially uncorrelated; $K(s,s')$ is then represented by a Brownian kernel[21,22]

$$K(s,s') \sim (s^{1/d} + s'^{1/d})^{d-2} [D(s) + D(s')], \tag{12}$$

where d is the system dimensionality and $D \propto s^{-\alpha}$ characterizes the dependence of island diffusion on s.

The exponent α describes the dominant microscopic mechanism underlying island diffusion. One important scaling relation in Smoluchowski ripening is between the growth exponent β' for the characteristic length scale $L \approx \xi \sim t^{\beta'}$, and α, given by[23]

$$\beta' = \frac{1}{2(\alpha+1)}. \tag{13}$$

For $d = 3$, we obtain for the kernel $K(s,s')$:

$$K(\lambda s, \lambda s') \sim \lambda^{1/3-\alpha} K(s,s'), \tag{14}$$

so that the number density n_s in the long time limit takes the following form:[12]

$$n_s(s,t) = A s^{\alpha - 1/3} \exp(-bs), \tag{15}$$

where $A \propto b^{\alpha+5/3}/\Gamma(\alpha+\frac{5}{3})$, $b = b_0 t^{-1/(\alpha+2/3)}$ for some constant b_0, and Γ is the gamma function. The probability density function P_s is therefore equal to

$$P_s = s n_s = A s^{\alpha+2/3} \exp(-bs), \tag{16}$$

which has a maximum at

$$\overline{s} = \frac{\alpha + 2/3}{b} \propto t^{\beta''}, \tag{17}$$

where $\beta'' = (\alpha + \frac{2}{3})^{-1}$.

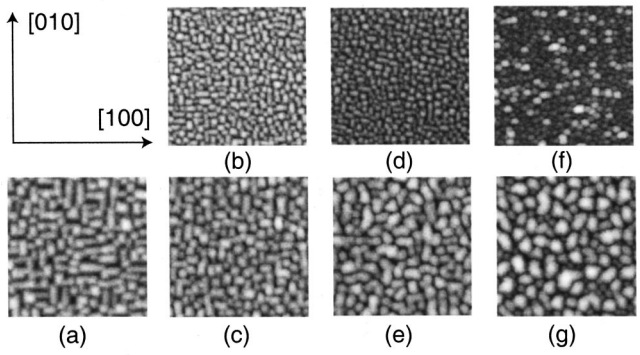

FIG. 2. 1.5 μm×1.5 μm AFM images of $Si_{1-x}Ge_x/Si(001)$ samples with varying Ge fractions and nominal thicknesses h_0. Sample group *W*: (a) *W*2: $x=0.3, h_0=20$ nm. Sample group *X*: (b) *X*1: $x=0.4, h_0=5$ nm; (c) *X*2: $x=0.4, h_0=20$ nm. Sample group *Y*: (d) *Y*1: $x=0.5, h_0=5$ nm; (e) *Y*2: $x=0.5, h_0=20$ nm. Sample group *Z*: (f) *Z*1: $x=0.7, h_0=5$ nm; (g) *Z*2: $x=0.7, h_0=20$ nm.

III. RESULTS AND DISCUSSION

$Si_{1-x}Ge_x$ single multilayer samples were grown on Si(001) substrates by ultrahigh vacuum chemical vapor deposition (UHV-CVD) at 525 °C with growth rate of 0.8 Å/s as described in detail elsewhere.[24] *Ex situ* atomic force microscopy (AFM) was used to obtain surface morphologies of samples as a function of Ge fraction and thickness. A lateral resolution of a few nanometers was achieved by using a Si_3N_4 cantilever tip. It was prevously demonstrated that negligible island shape distortion results from such measurements, compared with *in situ* measurements.[25]

Clipped images from height-mode 5 μm×5 μm AFM images are shown in Fig. 2. At the lowest misfit strain ($x=0.3$) and with nominal thickness $h_0=5$ nm; no island formation is observed, while at $h_0=20$ nm islands form and align themselves along elastically soft [100] and [010] directions [see Fig. 2(a)]. Flat square and rectangular islands that coexist in Fig. 2(b) can also be seen in Fig. 2(d), although they transform into hut-shaped islands with an average slope of 11.3° in Figs. 2(c) and 2(e), consistent with {501}-type facets.[25] Interestingly, we find from the surface slope histogram of sample *W*2 that hut-shape islands seem to be present in Fig. 2(a). In contrast, the highest value of slope in Fig. 2(b), for example, is only about 6°. Whereas the island morphologies can be related to one another in the cases of $x=0.3-0.5$, it is not the case at the largest misfit strain ($x=0.7$). We show in Sec. III A that the image sequence of samples $X1\rightarrow Y1\rightarrow X2\rightarrow Y2$ agrees with the sequence of their corresponding values of $|\langle h\rangle - h_p|$. We observe more isotropic (circular) flat islands of two different average sizes shown in Fig. 2(f), which transform into large domes with increasing layer thickness in Fig. 2(g); we find no hut-shaped islands at the highest misfit strain. Transmission electron microscopy studies of these samples show that faulted dislocation loops are found below island perimeters for sample *Z*2.[9]

A. Smoluchowski ripening: Results

Island morphologies shown in Fig. 2 strongly suggest coalescence is occuring, amalgamating islands into a cellular network without a significant island density loss. This behavior differs from that expected for Ostwald ripening, i.e., where atoms from smaller islands detach and diffuse on the surface, condensing on larger islands.[26] The overall effect of Ostwald ripening is the growth of larger islands at the expense of smaller islands. Light scattering spectroscopy of $Si_{0.8}Ge_{0.2}/Si(001)$ islands grown at 755 °C also found the nonoccurence of capillary-driven Ostwald ripening.[14] Our lower growth temperature further restricts the possibility of adatom diffusion needed for Ostwald ripening mechanism. In addition, higher Ge fractions in our samples introduce higher compressive lattice mismatch strains, thus producing a highly stressed region region around the island perimeter, where a topographical discontinuity with a flat wetting layer is located.

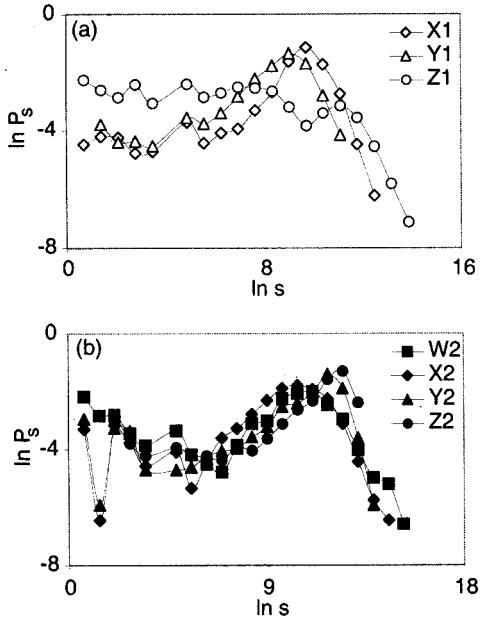

FIG. 3. Probability density functions P_s for (a) 5 nm and (b) 20 nm nominal thickness samples.

The probability density functions P_s for the samples studied are shown in Fig. 3. The shapes of P_s in Fig. 4 agree qualitatively with the so-called static coalescence model,[27] in which a power-law decay dominating for small-sized islands is superimposed on a monodispersed bell-shaped distribution peaked at large-sized island. Numerical simulations based on a *static* fusion of two droplets into a single droplet without volume loss demonstrate the applicability of scaling laws.[27] To determine the presence of scale invariance in P_s, the behavior of the probability density function needs to be determined near the critical state (i.e., $\langle h\rangle \approx h_p$). The scale invariance is characterized by a single characteristic length scale, i.e., the mean island size. Therefore, first the mean island size *S* is measured as defined in Eq. (2). Following common practice, we assume that *S* behaves as the correlation length ξ, in order to scale the distribution function $f(s/S)\sim f(s/\xi)$.[27] The correlation length ξ is computed from the height-height and the slope-slope correlations, respectively, defined as

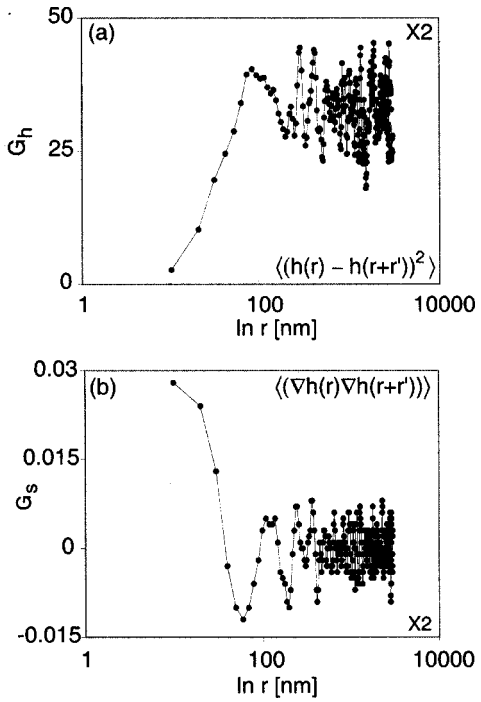

FIG. 4. Typical plots of (a) $G_h(r)$ and (b) $G_s(r)$. Shown are from sample $X2$. The correlation length ξ in $G_h(r)$ is taken to be the distance r where saturation begins, while ξ is taken to be the first zero of $G_s(r)$.

$$G_h(\mathbf{r},t)=\langle[h(\mathbf{r},t)-h(\mathbf{r}+\mathbf{r}',t)]^2\rangle, \tag{18}$$

$$G_s(\mathbf{r},t)=\langle\nabla h(\mathbf{r},t)\nabla h(\mathbf{r}+\mathbf{r}',t)\rangle, \tag{19}$$

and performed at equal times in order to obtain two different, independent values of ξ. This is because there are several available measures for ξ,[6,28,29] and at least two measurements are required to eliminate measurement bias. Typical plots for $G_h(r)$ and $G_s(r)$ are shown in Fig. 4. We summarize our results for S and ξ in Table I.

From the data for correlation length in Table I, the images should be organized in the following order: $X1\rightarrow Y1\rightarrow X2\rightarrow Y2$ based on the monotonous increase of ξ for these samples. This sequence is also consistent with their respective value of $\langle h\rangle - h_p$, as listed in Table II. Sample $W2$, on the other hand, gives a correlation length of ξ=49 nm and a

TABLE I. Measured mean island size S, median island size $\overline{s}$, and correlation length ξ obtained from $G_h(r)$ and $G_s(r)$.

Sample	S (nm^3)	$\overline{s}$ (nm^3)	ξ [nm] {from $G_h(r)$}	ξ [nm] {from $G_s(r)$}
$W2$	74 195	65 536	49	43
$X1$	19 161	16 384	34	22
$X2$	56 872	32 768	42	37
$Y1$	9991	8192	36	29
$Y2$	101 937	131 072	52	52
$Z1$	14 106	2048, 65 536[a]	42	39
$Z2$	160 666	262 144	80	39

[a]Sample $Z1$ has a bimodal distribution.

TABLE II. Important parameters used in statistical analysis: average height $\langle h\rangle$; standard deviation of height histogram ϱ; critical thickness h_c; nominal thickness h_0. Constants for the analysis are: the first-layer percolation threshold θ_p=0.6 ML, lattice constants for Ge and Si: a_{Ge}=0.565 nm and a_{Si}=0.543 nm, respectively. All parameters below are presented in monolayers.

Sample	$\langle h\rangle$	ϱ	h_c	h_0
$W2$	88.8	24.0	138.3	145.6
$X1$	52.2	14.5	29.0	36.2
$X2$	110.9	31.2	29.0	145.0
$Y1$	55.6	17.3	14.4	36.1
$Y2$	153.1	49.8	14.4	144.4
$Z1$	63.0	25.1	5.7	35.8
$Z2$	162.6	69.5	5.7	143.3

negative value of $\langle h\rangle - h_p$, which is not consistent with this sequence. In addition, we also find that sample group Z cannot be grouped together with sample groups X and Y. Sample $Z1$ develops a bimodal size distribution as evident from Fig. 3, indicating the presence of a metastable state as characterized by the smaller distribution peak. The transient nature of this state is apparent from its disappearance in sample $Z2$, where a unimodal size distribution is recovered. This may help explain discrepancies with the initial grouping above, where sample $Z2$ is excluded due to a possibly different kinetic pathway due to the formation of dislocations in sample $Z2$. We speculate that the origin for the metastable state is related to a strain-induced shape transition, mediated by dislocation formation. This dislocation-mediated shape transition is analogous to the pyramid-to-dome shape transition in Ge/Si(001) islands,[30] except that we did not observe a trimodal distribution.

In order to determine the coarsening of S as a function of time, we use the relation $\langle h\rangle\approx Ft$ and shift $\langle h\rangle$ by h_p as defined in Sec. II. Thus, we assume that $S\propto t^{\beta}$, where β is growth exponent. Table II lists the important parameters for the statistical analysis. Pure Si and Ge have a diamond lattice, so that 1 ML=a/4 for the [001] direction, where a is the corresponding lattice constant. For $\mathrm{Si}_{1-x}\mathrm{Ge}_x$, we assume Vegard's law for $a(x)$, giving

$$h(x)[\mathrm{ML}]=\frac{4h(x)[\mathrm{nm}]}{xa_{\mathrm{Ge}}+(1-x)a_{\mathrm{Si}}},$$

where a_{Ge}=0.565 nm and a_{Si}=0.543 nm. The critical thickness h_c for each sample (except for sample $W2$) is consistently below the average height $\langle h\rangle$, and even below $\langle h\rangle - \varrho$ as well, where ϱ is the standard deviation of height histogram. Since h_c is the height at which 2D islands start forming (and subsequently transform into 3D islands) samples, except $W2$, are already above percolation threshold $h_p=h_c+\theta_p$ with respect to the 2D islands. Hence, we do not use measurement results from sample $W2$. Figure 5 displays the dependence of S on $\langle h\rangle - h_p$, giving a growth exponent of β=1.30±0.20, while Fig. 6 shows the dependence of ξ values on time t: $\xi\propto t^{\beta'}$, giving β'=0.37±0.05 and 0.41 ±0.02 from $G_h(\mathbf{r},t)$ and $G_s(\mathbf{r},t)$, respectively. For a

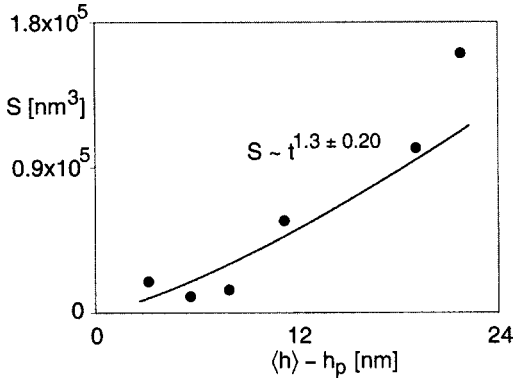

FIG. 5. The behavior of mean island size S as a function of $|\langle h\rangle - h_p|$ gives $\beta = 1.30 \pm 0.2$.

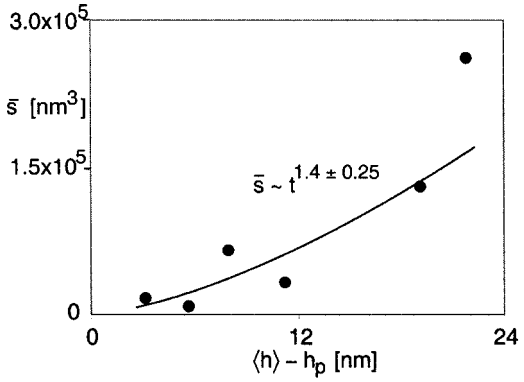

FIG. 7. The behavior of the median island size $\bar{s}$ as a function of $|\langle h\rangle - h_p|$, giving $\beta'' = 1.4 \pm 0.25$.

d-dimensional island, we assume that $S \sim \xi^d$, giving $\beta' \sim \beta^{1/d}$. The results show that $d \gtrsim 3$. The value of $\beta' \approx 0.4$ is unexpected for Ostwald ripening, where $\beta' = \frac{1}{3}$ for both two and three-dimensional systems.[31,32] However, stronger evidence for the presence of coalescence ripening, rather than Ostwald-type ripening, lies with the island morphologies shown in Fig. 2.

Light scattering spectroscopy of $Si_{0.8}Ge_{0.2}/Si(001)$ islands gives another evidence that Ostwald ripening, when solely driven by surface energy minimization, does not occur, even during growth at 755 °C.[14] It was also found that the average island size grows superlinearly with time. Floro and co-workers[14] treated this deviation fom the standard Oswald ripening behavior by adding an elastic interaction term obtained from finite element calculations to the coarsening model.[30] Our samples were grown at 525 °C, which strongly

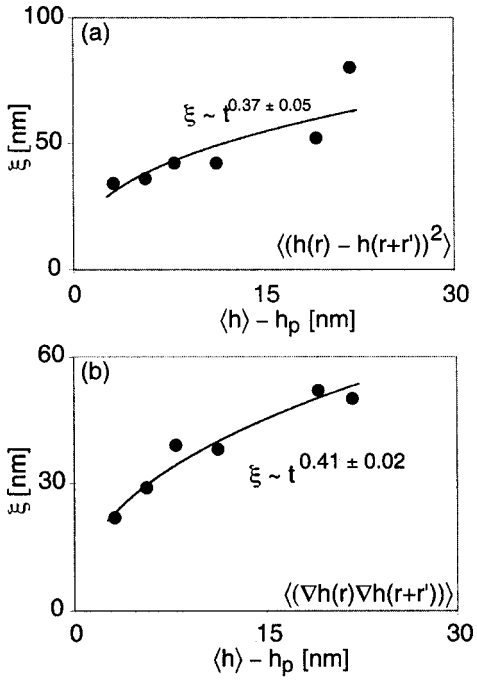

FIG. 6. The behavior of the correlation length ξ as a function of $|\langle h\rangle - h_p|$ as defined from (a) $G_h(\mathbf{r},t)$ and (b) $G_s(\mathbf{r},t)$, giving $\beta' = 0.37 \pm 0.05$ and 0.41 ± 0.02, respectively.

limits adatom diffusion necessary for Ostwald-ripening-type mechanism. In addition, Ge fractions in our samples are 0.3–0.7, which create higher lattice mismatch strains, thus increasing strain-induced energy barriers around the island boundary with the wetting layer.

Using Eq. (13), we find that $\alpha = 0.28 \pm 0.20$. Hence, the island diffusion constant D has a weak dependence on island size s: $D \sim s^{-0.28 \pm 0.20}$. As a comparison, $\alpha \approx 1.5$ when an island diffuses by having atoms hopping along its periphery, and $\alpha \approx 0.5$ for island diffusion governed by a random exchange (evaporation-condensation) mechanism with the surrounding two-dimensional gas phase.[20] In the latter case, the growth exponent is $\beta' \approx 0.33$, which agrees with that of Ostwald-type ripening whose underlying mechanism is evaporation of atoms from smaller islands and their condensation onto larger islands.

The value for $\alpha = 0.28 \pm 0.20$ is close to that reported by Sholl and Skodje.[23] Their Monte Carlo simulations of Xe clusters diffusing on Pt(111) gave $\alpha = 0.35 \pm 0.12$, which was attributed to multiple barriers a Xe atom must overcome before escaping completely from the cluster. Atoms in a semiconductor island are tightly bound due to their covalent bonding; Si and Ge atoms comprising a $Si_{1-x}Ge_x$ island are much more immobile than atoms in a metal cluster. By contrast, diffusion of two-dimensional Ag clusters on Ag(001) can produce $\alpha \approx 1.75$.[33] It is postulated that the multiple barriers imposed on Si and Ge atoms, originate from the inverse process of sequential incorporation of atoms at step edges due to high stress concentration around an island terrace.[9] This inverse process limits the escape rate of Si and Ge atoms from a $Si_{1-x}Ge_x$ island, making the island much less mobile and resulting in a weak dependence of the island diffusion constant on island size.

Using Eq. (17), we obtain $\beta'' = (\alpha + \frac{2}{3})^{-1} = 1.1 \pm 0.22$. We can independently verify the dependence of $\bar{s}$ on t by plotting the median values of P_s as a function of $|\langle h\rangle - h_p|$ as shown in Fig. 7, giving an exponent $\beta'' = 1.4 \pm 0.25$. These two values give reasonable agreement despite (i) simplifying assumptions in obtaining n_s (Ref. 12) and (ii) the probability density functions P_s in Fig. 3, have a power-law decay for small s.

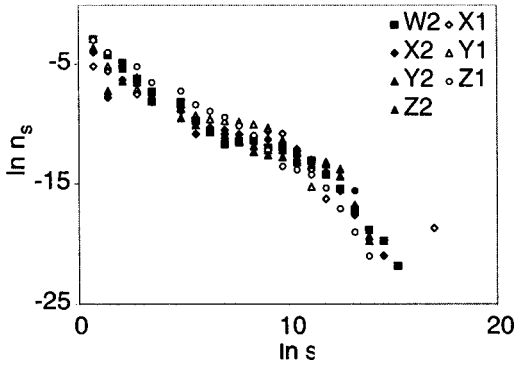

FIG. 8. The number densities n_s per lattice site as a function of island size s as defined in Eq. (4).

B. Random percolation: Results

Since $\alpha+\frac{2}{3}>0$, the dependence of P_s on s [i.e., Eq. (16)] results in a maximum probability at $\overline{s}=(\alpha+\frac{2}{3})b^{-1}$. Random percolation process, however, results in only a subexponential decay once the average film thickness $\langle h\rangle$ exceeds the percolation threshold h_p.[6] The probability distribution functions shown in Fig. 3 suggest the presence of both of these processes. We therefore propose that by combining them,

$$P_s = As^{\alpha+2/3}\exp(-bs) + Cs^{-\sigma} f(s^{1/(\nu\tau)}|\langle h\rangle - h_p|), \qquad (20)$$

we may be able to fit the measured probability density functions. The number density $n_s = P_s/s$ is therefore given by

$$n_s = As^{\alpha-1/3}\exp(-bs) + Cs^{-\sigma-1} f(s^{1/(\nu\tau)}|\langle h\rangle - h_p|). \quad (21)$$

The unknown parameters in Eqs. (20) and (21) are A, b_0, and C since both $\sigma=1.2$ and $\Delta=\nu\tau=\frac{20}{9}\approx 2.22$ are known values from the $d=3$ percolation problem.[6,16] We assess the validity of Eq. (20) by considering the number density n_s of islands per lattice site, which is shown in Fig. 8. Power-law decay clearly dominates in the small size limit, while the distribution peak, represented by a gentle hump located at $\ln s\approx 11$, occurs in the large size limit. The hump signifies that $\alpha>\frac{1}{3}$ since the contrary, i.e., $\alpha\lesssim\frac{1}{3}$, would yield a monotonously decaying profile for n_s as $s\to\infty$. We recall that we obtain $\alpha=0.28\pm 0.20$ from mean island size and correlation lengths data.

The results indicate that the *simultaneous* presence of random percolation and Smoluchowski ripening destroys the scale invariance of n_s, although it is demonstrated in Fig. 8 that they operate on different size scales. We also learn that the scaling function $f(s^{1/\Delta}|\langle h\rangle - h_p|)$ can be approximated by a power-law function

$$f(s^{1/\Delta}|\langle h\rangle - h_p|) \approx s^{\omega/\Delta}|\langle h\rangle - h_p|^{\omega} \text{ for small } s, \quad (22)$$

such that $(\omega/\Delta)<\sigma+1$, in order to ensure that the number density n_s still produces a power-law decay, as evident from Fig. 8.

To recover the scaling function for random percolation $f(s^{1/\Delta}|\langle h\rangle - h_p|)$ we rescale the number densities of Fig. 8 using $\sigma=1.2$ and $\Delta=\nu\tau=2.22$, as shown in Fig. 9. Sample $W2$ is separated from the others since it corresponds to below-percolation-threshold behavior. Fitting the scaling

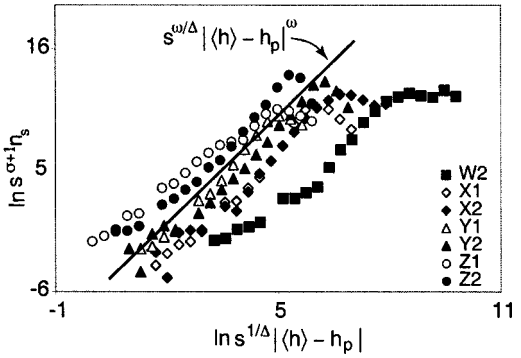

FIG. 9. Rescaling the number densities n_s fails to demonstrate the scale-invariance property of $f(s^{1/(\nu\tau)}|\langle h\rangle - h_p|)$, due to the simultaneous presence of random percolation and Smoluchowski ripening. However, it can still be approximated with $f(x)\propto x^{-\omega}$ by considering its $x\to 0$ behavior.

function approximation in Eq. (22) to each of the rescaled curves, gives $\omega=3.0\pm 0.38$, and so the number density n_s assumes the following expression for the small s limit:

$$n_s \propto s^{-\sigma-1+\omega/\Delta}|\langle h\rangle - h_p|^{\omega},$$
$$\propto s^{-0.90\pm 0.15}|\langle h\rangle - h_p|^{3.0\pm 0.38}, \qquad (23)$$

whose exponent $0.90\pm 0.15=\sigma+1-(\omega/\Delta)$ is comparable with the power-law exponent of 0.94 ± 0.14, obtained directly by fitting a power-law function to the n_s curves in Fig. 8. This exercise shows that the value for ω is consistent with random percolation at $d=3$.

When the ripening process is due only to random percolation, then the kth moments of distribution near the critical state can be approximated by

$$M_k = \frac{\sum_s s^{k+1}P_s(s)}{\sum_s s^k P_s(s)},$$
$$\simeq \frac{\int_0^{\infty} ds s^{k+1-\sigma} f(s\xi^{-\tau})}{\int_0^{\infty} ds s^{k-\sigma} f(s\xi^{-\tau})},$$
$$\simeq \frac{\xi^{\tau(k+1-\sigma)+\tau}\int_0^{\infty} dz\, z^{k+1-\sigma} f(z)}{\xi^{\tau(k-\sigma)+\tau}\int_0^{\infty} dz\, z^{k+1-\sigma} f(z)}, \qquad (24)$$

where the last expression is evaluated by substituting $s = s\xi^{-\tau}$. Since the integrals are functions of k only when $f(z)$ decays faster than z^{-1},

$$M_k \simeq C_k \xi^{\tau} \sim |\langle h\rangle - h_p|^{-\Delta}, \qquad (25)$$

where $\Delta=\nu\tau$. Hence, Δ must be constant for any $k\geqslant 1$ for a pure random percolation process.[6] We do not see any power-law behavior in $M_{k\leqslant 3}$ as a function of $(\langle h\rangle - h_p)$; for example, M_1 suggests a logarithmic behavior as shown in Fig.

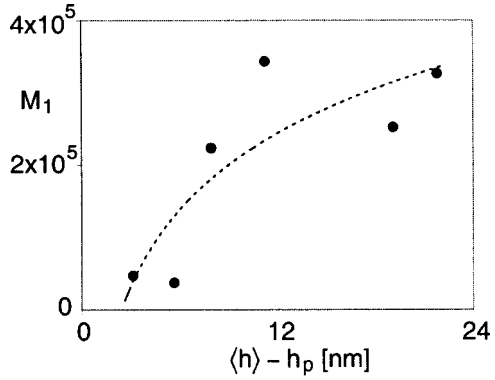

FIG. 10. First moments of the distribution do not exhibit a power-law behavior. The dashed curve is the fitted logarithmic curve.

10, implying that $f(z)$ is no longer scale invariant. The slow decay of n_s already indicates this behavior. The breakdown of scale invariance will cause the integrals to diverge in the limit $z\rightarrow\infty$ as more islands become larger due to Smoluchowski ripening. From our correlation lengths data, we also find little evidence that $\xi\rightarrow\infty$, causing the term $z^{k+1-\sigma}$ to become unbounded as $s\rightarrow\infty$.

C. Distribution densities

To summarize results from Smoluchowski ripening and random percolation process, we list the values of relevant exponents below:

$$\alpha=0.28\pm0.20,\quad \omega=3.0\pm0.28,\quad \sigma=1.2,\quad \Delta=\nu\tau=2.22, \tag{26}$$

where the last two values are critical exponent values for percolation at $d=3$. We also recall that $\alpha>\frac{1}{3}$ due to the presence of the gentle hump in n_s; thus, we take $\alpha\equiv0.4$ to fit the distribution functions with these exponents:

$$\begin{aligned} P_s &\approx As^{\alpha+2/3}\exp(-bs)+Cs^{-\sigma+(\omega/\Delta)}|\langle h\rangle-h_p|^{\omega}, \\ &\approx As^{1.07}\exp(-bs)+Cs^{0.10\pm0.15}|\langle h\rangle-h_p|^{3.0\pm0.38}, \end{aligned} \tag{27}$$

where the adjustable parameters are A and C. The constant b is given by Eq. (17). We note that the second term gives a decaying profile if the exponent is less than zero.

Figure 11 demonstrates the goodness of fit for the proposed distribution function in Eq. (27) to all but sample $W2$. The fitted curve shown by open squares agrees well in five cases, except for sample $Z1$, where significant bimodality occurs. Each distribution peak is controlled by Smoluchowski ripening, although it is not clear from our model the nature of metastable islands exhibited in sample $Z1$. The pairwise collision assumption in the Smoluchowski ripening process provides a very good fit to the distributions. Random percolation is dominant in the small island size range, below $s\approx250$ nm^3, and to some degree in the large size limit. We use the range of $\sigma-(\omega/\Delta)=0.03-0.05$, which is within the range for $\sigma-(\omega/\Delta)=-0.10\pm0.15$.

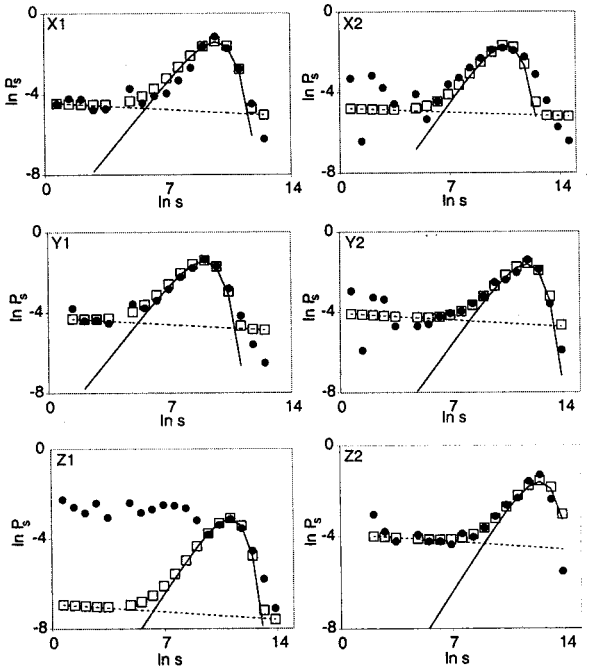

FIG. 11. Fitting curves for the probability distribution functions P_s are obtained by adding the contributions from Smoluchowski ripening (solid curves) and random percolation (dashed curves) as indicated by open squares. Good agreement is obtained for six samples, except sample $Z1$ that has a bimodal distribution. Here, the exponent $\sigma+(\omega/\Delta)=0.03-0.05$, which is within its obtained value of 0.15 ± 0.17, and the other parameters are listed in Eq. (26). Sample $W2$ is not included as it is below percolation threshold.

The constant A is shown to have the following expression:[12]

$$A\propto b^{\alpha+5/3}\propto t^{-(\alpha+5/3)/(\alpha+2/3)}. \tag{28}$$

for Smoluchowski ripening at $d=3$ as obtained in Sec. III A. For $\alpha=0.28\pm0.20$, we have $A\propto t^{-2.03\pm0.22}$. Fitting the constants A as a function of $t\propto\langle h\rangle-h_p$, i.e., $A\propto t^a$, we obtain $a=-1.61\pm0.44$ as displayed in Fig. 12. This provides fur-

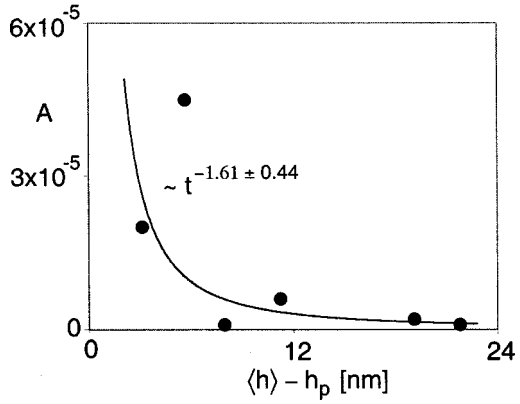

FIG. 12. The dependence of A on $t\propto|\langle h\rangle-h_p|$: $A\propto|\langle h\rangle-h_p|^a$, produces $a=-1.61\pm0.44$, within the predicted value of 2.03 ± 0.22.

ther evidence that the pairwise collision assumption is adequate.

IV. SUMMARY AND CONCLUSIONS

The probability density functions of ripened $Si_{1-x}Ge_x/Si(001)$ islands are shown to have two components. First, the random percolation process that describes uncorrelated island ripening operates in the small size limit. The critical exponents from our measurements agree with $d=3$ percolation, which provides indirect evidence that the ripening process cannot be adequately described by a mean-field description. This is because the upper critical dimension for random percolation is $d_u=6$,[6] so that for $d>6$, the mean-field description, whereby strong interactions producing spatially varying inhomogeneities are suppressed, is valid. The additional mechanism required to fully describe the data is Smoluchowski ripening, in which island coalescence occurs via pairwise collisions. We find that the distribution peaks can be attributed largely to the latter mechanism that dominates in the large size limit. It was found that the scaling exponents for this latter mechanism do not agree with the corresponding mean-field values.

The simultaneous presence of these two mechanisms breaks down the scaling laws, which are commonly obeyed in both submonolayer and preripening multilayer islands. This may be traced to the fact that in submonolayer islands, the island size distribution decays exponentially,[2] in agreement with the exponential decay in percolation at coverages below the first-layer percolation threshold.[6] This may further indicate that island-island interactions are negligible during submonolayer growth. During island growth in the preripening multilayer stage, it may be possible for the islands to reach a metastable equilibrium, which is evident in the case of the largest Ge fraction sample. The presence of such a metastable state may force the islands to reach relatively uniform sizes. However, we find that dislocation formation can quickly dissipate this state, followed by ripening of these dislocated islands. Without such a metastable state, the island size distribution decays subexponentially, hence degrading the size uniformity. This occurs in samples with smaller Ge fractions. Another route to ensure relatively uniform sizes is to terminate the growth of 3D islands before the percolation threshold h_p is reached. As the islands grow, Smoluchowski ripening provides a second avenue for the islands to reach a relatively uniform size distribution.

It is demonstrated that in order to have relatively uniform small island sizes, a metastable state is required. A slow decay of size distributions in the small size limit (in multilayer samples) indicates that it is difficult to achieve a high degree of size uniformity without the existence of a metastable state. Although Smoluchowski ripening may provide a size narrowing mechanism, the average size at this stage may be already too large for some technological applications, such as in quantum dot lasers. For other applications that can utilize large island sizes, the Smoluchowski ripening mechanism can actually enhance size uniformity by developing a continuous cellular network.

We have demonstrated the applicability of an effective average film height $\langle h\rangle - h_p$ to represent the time variable t in analyzing the size distributions. This analogy is taken from the percolation theory, and can be directly transfered to the Smoluchowski ripening model. This provides an alternative way to analyze the dependence of island size distributions on misfit strain ε through the critical thickness h_c that rescales the time variable t. This may provide an exciting development in further understanding the evolution and stability issues for 3D island formation.

Random percolation process demands that the deposited particles be immobile once they arrive on the surface, although it has been shown that percolation threshold changes little when they diffuse.[1,8] Nevertheless, a large adatom diffusion current at elevated growth temperatures may change the nature of 3D percolation; our samples were grown at relatively low temperatures. The interplay among shapes, heights, and sizes of 3D islands due to growth parameters requires further studies. One interesting development in this direction is, for example, given by a study of correlated granular percolation.[34] By specifying the maximum 2D cluster size, there is a concomitant maximum surface site density, indicating a balance between surface tension and bulk elastic energy density of the cluster. Another direction is combining our work with scaling properties of surface roughening[8] that leads to compact 3D islands.[35]

One fundamental issue worth investigating is thus determining the range of applicability of the 3D random percolation to the 3D island size distributions. Concretely, the interplay between the island shape and height distributions in determining the size distributions might be investigated to gain a comprehensive understanding for clustering mechanisms in ripened islands. In these regards, we hope that our study would stimulate more detailed investigations, incorporating these issues, in the future.

ACKNOWLEDGMENTS

The authors thank D. D. Perović and B. Bahierathan for providing excellent samples and for many valuable discussions. A.B. thanks S. V. Nair for the critical reading of our manuscript. The authors gratefully acknowledge the financial support of the Natural Science and Engineering Research Council (NSERC), and the Mathematics of Information Technology and Complex Systems (MITACS). A.B. was also supported by the University of Toronto.

[1] J. G. Amar, F. Family, and P.-M. Lam, Phys. Rev. B **50**, 8781 (1994).

[2] J. G. Amar and F. Family, Phys. Rev. Lett. **74**, 2066 (1995).

[3] M. C. Bartelt and J. W. Evans, Surf. Sci. **298**, 421 (1993).

[4] Y. Ebiko, S. Muto, D. Suzuki, S. Itoh, K. Shiramine, T. Haga, Y. Nakata, and N. Yokoyama, Phys. Rev. Lett. **80**, 2650 (1998).

[5] V. Bressler-Hill, S. Varma, A. Lorke, B. Z. Nosho, P. M. Petroff, and W. H. Weinberg, Phys. Rev. Lett. **74**, 3209 (1995).

[6] G. Grimmett, *Percolation* (Springer, Berlin, 1989).
[7] V. A. Shchukin and D. Bimberg, Rev. Mod. Phys. **71**, 1125 (1999).
[8] F. Family, Physica A **266**, 173 (1999).
[9] D. D. Perović, B. Bahierathan, H. Lafontaine, D. C. Houghton, and D. W. McComb, Physica A **239**, 11 (1997).
[10] R. M. Tromp, F. M. Ross, and M. C. Reuter, Phys. Rev. Lett. **84**, 4641 (2000).
[11] B. J. Spencer, P. W. Voorhees, and S. H. Davis, J. Appl. Phys. **73**, 4955 (1993).
[12] D. S. Sholl and R. T. Skodje, Physica A **231**, 631 (1996).
[13] R. J. Barel, G. R. Carlow, M. Zinke-Allmang, Y. Wu, and T. Lookman, Physica A **239**, 53 (1997).
[14] J. A. Floro, M. B. Sinclair, E. Chason, L. B. Freund, R. D. Twesten, R. Q. Hwang, and G. A. Lucadamo, Phys. Rev. Lett. **84**, 701 (2000).
[15] J. W. Evans and M. C. Bartelt, J. Vac. Sci. Technol. A **12**, 1800 (1994).
[16] D. Stauffer, *Introduction to Percolation Theory* (Taylor & Francis, London, 1985).
[17] D. Leonard, K. Pond, and P. M. Petroff, Phys. Rev. B **50**, 11 687 (1994).
[18] T. Pinnington, Y. Levy, J. A. MacKenzie, and T. Tiedje, Phys. Rev. B **60**, 15 901 (1999).
[19] G. S. Solomon, J. A. Trezza, and J. S. Harris, Jr., Appl. Phys. Lett. **66**, 991 (1995).
[20] C. R. Stoldt, C. J. Jenks, P. A. Thiel, A. M. Cadilhe, and J. W. Evans, J. Chem. Phys. **111**, 5157 (1999).
[21] S. Chandrasekhar, Rev. Mod. Phys. **15**, 1 (1943).
[22] K. Kang, S. Redner, P. Meakin, and F. Leyvraz, Phys. Rev. A **33**, 1171 (1986).
[23] D. S. Sholl and R. T. Skodje, Phys. Rev. Lett. **75**, 3158 (1995).
[24] H. Lafontaine, D. C. Houghton, D. Elliot, N. L. Rowell, J.-M. Baribeau, S. Laframboise, G. I. Sproule, and S. J. Rolfe, J. Vac. Sci. Technol. B **14**, 1675 (1996).
[25] G. Medeiros-Ribeiro, A. M. Bratkovski, T. I. Kamins, D. A. A. Ohlberg, and R. S. Williams, Science **279**, 353 (1998).
[26] M. Zinke-Allmang, L. C. Feldman, and M. H. Grabow, Surf. Sci. Rep. **16**, 377 (1992).
[27] F. Family and P. Meakin, Phys. Rev. Lett. **61**, 428 (1988).
[28] A. Pimpinelli and J. Villain, *Physics of Crystal Growth* (Cambridge University Press, Cambridge, 1998).
[29] A.-L. Barabási and H. E. Stanley, *Fractal Concepts in Surface Growth* (Cambridge University Press, Cambridge, 1995).
[30] F. M. Ross, J. Tersoff, and R. M. Tromp, Phys. Rev. Lett. **80**, 984 (1998).
[31] P. W. Voorhees, J. Stat. Phys. **38**, 232 (1985).
[32] C. Sagui and R. C. Desai, Phys. Rev. Lett. **74**, 1119 (1995).
[33] J.-M. Wen, S.-M. Chang, J. W. Burnett, J. W. Evans, and P. A. Thiel, Phys. Rev. Lett. **73**, 2591 (1994).
[34] T. Odagaki, H. Kawai, and S. Toyofuku, Physica A **266**, 49 (1999).
[35] J. Tersoff and F. K. LeGoues, Phys. Rev. Lett. **72**, 3570 (1994).